Chemistry & Biology 13, 261–268, March 2006 ©2006 Elsevier Ltd All rights reserved DOI 10.1016/j.chembiol.2005.12.008

Stable Benzotriazole Esters as Mechanism-Based Inactivators of the Severe Acute Respiratory Syndrome 3CL Protease

Chung-Yi Wu,[1,2] Ke-Yung King,[1] Chih-Jung Kuo,[1,3] Jim-Min Fang,[1,4] Ying-Ta Wu,[1] Ming-Yi Ho,[1] Chung-Lin Liao,[1] Jiun-Jie Shie,[1] Po-Huang Liang,[1,*] and Chi-Huey Wong[1,2,4,*]

[1] The Genomics Research Center and Institute of Biological Chemistry
Academia Sinica No. 128
Academia Road Section 2
Nan-Kang
Taipei, 115
Taiwan

[2] Department of Chemistry and Skaggs Institute for Chemical Biology
The Scripps Research Institute
10550 North Torrey Pines Road
La Jolla, California 92037

[3] Taiwan International Graduate Program
Academia Sinica
Nan-Kang
Taipei, 115
Taiwan

[4] Department of Chemistry
National Taiwan University
Taipei, 106
Taiwan

Summary

Severe acute respiratory syndrome (SARS) is caused by a newly emerged coronavirus that infected more than 8000 individuals and resulted in more than 800 fatalities in 2003. Currently, there is no effective treatment for this epidemic. SARS-3CL^{pro} has been shown to be essential for replication and is thus a target for drug discovery. Here, a class of stable benzotriazole esters was reported as mechanism-based inactivators of 3CL^{pro}, and the most potent inactivator exhibited a k_{inact} of 0.0011 s^{-1} and a K_i of 7.5 nM. Mechanistic investigation with kinetic and mass spectrometry analyses indicates that the active site Cys145 is acylated, and that no irreversible inactivation was observed with the use of the C145A mutant. In addition, a noncovalent, competitive inhibition became apparent by using benzotriazole ester surrogates in which the bridged ester-oxygen group is replaced with carbon.

Introduction

Severe acute respiratory syndrome (SARS), a newly emerged infectious disease, first occurred in Guandong (China) in November of 2002 and spread through many countries in 2003; it reemerged in China in December 2003 and in the spring of 2004. This disease is caused by infection with a novel human coronavirus (SARS-CoV) [1–3], which affected more than 8000 individuals across 32 countries and resulted in more than 800 fatalities in 2003 [4–6]. The origin of SARS-CoV is unclear, though studies on the molecular evolution of SARS-CoV indicate that the virus may have emerged from nonhuman species [7]. At present, no efficacious therapy for SARS is available. Therefore, a search for effective antivirals for the SARS-CoV is of current interest.

SARS coronavirus is a positive-strand RNA virus that encodes two polyproteins, pp1a and pp1ab [8–10], for further proteolytic processing to provide the functional proteins for viral propagation. These processes are mediated primarily by the main protease (M^{pro}), known as dimeric chymotrypsin-like protease (3CL^{pro}) [11–13]. The active site of 3CL^{pro} contains Cys145 and His41, constituting a catalytic dyad in which the cysteine thiol functions as the nucleophile in the proteolytic process [11–13]. Due to its essential role in viral replication, the protease is an attractive target for the development of therapeutics against SARS.

So far, only a few inhibitors of 3CL^{pro} have been reported, including the HIV protease inhibitor TL-3 [14], zinc-conjugated compounds [15], aryl boronic acids analogs [16], a quinolinecarboxylate derivative [17], a thiophenecarboxylate [18], phthalhydrazide-substituted keto-glutamine analogs [19], and anilides [20]. However, none of these inhibitors exhibits activities in the low nanomolar range, and no preclinical studies were reported.

As a part of our efforts directed toward the development of potent anti-SARS agents, we report here the discovery of a new class of mechanism-based irreversible inactivators with inhibition constants in the nanomolar range, by using the strategy of combinatorial reaction in microtiter plates followed by screening in situ [21–23]. This approach relies on the use of high-yield organic reactions that can be carried out in water or water-miscible, nontoxic solvents on microscales without protecting groups, allowing the product to be assayed directly in situ without isolation and purification. Using this approach, one can quickly modify a lead compound with a small set of building blocks to identify an optimal inhibitor.

Results and Discussion

Previously [14], we have reported that the HIV protease inhibitor Lopinavir (Figure 1) also inhibits 3CL^{pro} with an IC_{50} of ~50 μM. In order to find more potent 3CL^{pro} inhibitors, a library of Lopinavir-like compounds was assembled by using either diamine **1** or amine **2** as the core structure [24] for reaction with various acids in microtiter plates followed by screening in situ (Figure 1). In a typical procedure [21–23], a library of 90 carboxylic acids (see the Supplemental Data available with this article online) (10 μmol each) in a microtiter plate was used to couple with amine **1** or **2** (10 μmol) in the presence of *N*,*N*-diisopropylethylamine (22 μmol) and 2-(1*H*-benzotriazole-1-yl)-1,1,3,3-tetramethyluronium hexafluorophosphate (HBTU, 11 μmol) in DMF (100 μl) for 4 hr. An aliquot of the product, based on a putative 100%

*Correspondence: phliang@gate.sinica.edu.tw (P.-H.L.); wong@scripps.edu (C.-H.W.)

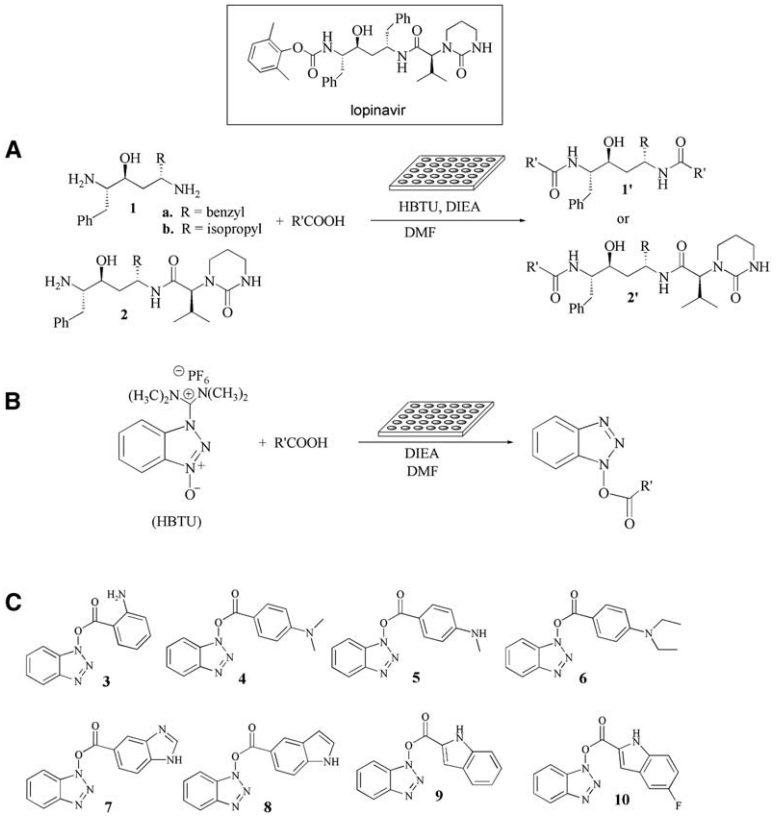

Figure 1. Microtiter Plate-Based Reactions and In Situ Screening

(A) Reactions of **1** or **2** with 90 acids in microtiter plates, followed by in situ screening for inhibitors of SARS-CoV $3CL^{pro}$.

(B) Reactions of HBTU and 90 acids in microtiter plates, followed by in situ screening for inhibitors of SARS-CoV $3CL^{pro}$.

(C) Molecular structures of inhibitors **3–10** against SARS-CoV $3CL^{pro}$.

conversion of starting materials, was taken and subjected to the $3CL^{pro}$ inhibition assay in a 20 mM Bis-Tris buffer (pH 7.0) at 25°C. To obtain the IC_{50} values, the initial velocities of the inhibited reactions with 50 nM of the protease and 6 μM of a fluorogenic substrate were plotted against different inhibitor concentrations. In this study, we noticed that the products derived from 2-aminobenzoic acid (well C9, IC_{50} = 0.2 μM), 4-(methylamino)benzoic acid (well D5, IC_{50} = 0.3 μM), 4-(dimethylamino)benzoic acid (well D6, IC_{50} = 0.5 μM), and 4-(diethylamino)benzoic acid (well D7, IC_{50} = 0.5 μM) showed the best inhibition and that the degree of inhibition was independent of the amine used.

In order to characterize the inhibitors, we attempted to separately prepare the pure amide derivatives, but we found that the amide formation was very slow, and that the intermediates benzotriazole esters **3**−**6** were isolated as major products from silica gel columns (the X-ray ORTEP structure of compound **4** is shown in the Supplemental Data). To our surprise, all of the Lopinavir-like compounds showed only modest inhibitory activities toward $3CL^{pro}$ ($IC_{50} \geq 10$ μM), whereas benzotriazole esters **3**−**6** showed high inhibition activities. To our knowledge, benzotriazole esters have been used as acylating agents and have never been found to be enzyme inhibitors. We then prepared a series of benzotriazole esters by condensation of HBTU with various carboxylic acids (Figure 1B), and we found that the benzotriazole esters derived from benzoic acid containing electron-withdrawing substituents, e.g., NO_2, CN, and CF_3, were susceptible to hydrolysis, whereas benzotriazole esters **3–6** and those with electron-donating groups were relatively stable in pH 5.0–8.0 over 24 hr at room temperature. The relative stability of each derivative depends on the p*K*a of the corresponding benzoic acid and basically follows the Hammett equation [25–27]. These stable benzotriazole esters, esters **3–10** (Figure 1C), were assayed, and their inhibition results against $3CL^{pro}$ are shown in Table 1.

Further study of the inhibition of benzotriazole esters **3–10** showed that there was a time-dependent decrease in enzyme activity as a function of the inhibitor concentration (e.g., the inhibition of compound **4**) (Figure 2A). In the presence of 1 mM DTT (dithiothreitol), the preincubation of enzyme with inhibitor did not affect the enzyme activity, indicating that DTT can protect the enzyme from inactivation (Figure 2B). These experiments indicate an irreversible mode of action and point to the active site Cys being involved in the inactivation process. The kinetic results for k_{inact} and K_i determinations of compound **4** are shown in Figures 2C and 2D (the detailed

Table 1. IC_{50}, K_i, k_{inact}, and CC_{50} of Benzotriazole Esters

Compounds	K_i (nM)	k_{inact} (s^{-1}) × 10^3	k_{inact}/K_i ($M^{-1}s^{-1}$) × 10^{-3}	CC_{50} (μM)
3	19.5	1.6	82.0	>100
4	17.4	1.3	74.7	>100
5	12.1	0.9	74.4	>100
6	11.1	0.8	72.1	>100
7	22.9	1.1	48.0	>100
8	7.5	1.1	146.7	>100
9	12.3	0.9	73.2	>100
10	13.8	1.2	86.9	>100

CC_{50}: The concentration that causes 50% cytotoxicity.

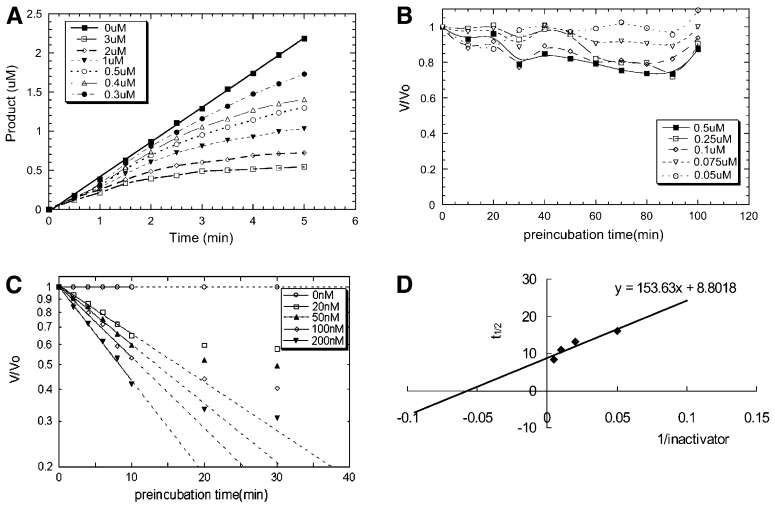

Figure 2. Kinetic Studies of Inhibitor **4** and SARS-CoV 3CL^{pro}

(A) The progress curves in the presence of 0.3–3.0 μM inhibitor for reactions initiated by adding enzyme (final concentration of 0.05 μM) into a mixture of substrate (6 μM) and inhibitor **4**. Over the entire 5 min time window, the uninhibited enzyme displayed a linear progress curve, whereas the inhibited enzyme with a different concentration of inhibitor showed a time-dependent reduction of activity.

(B) The same experiments as performed in (A), but with 1 mM DTT in the preincubation mixture.

(C) Preincubation time dependence of the fractional velocity of the protease-catalyzed reaction in the presence of 0.02–0.2 μM time-dependent inhibitor **4**.

(D) Kitz and Wilson replot of the half-life ($t_{1/2}$) of enzyme inactivation as a function of the reciprocal of the slow inactivator concentration. The k_{inact} is 0.0013 s^{-1} and K_i is 17.4 nM for the time-dependent inactivator **4** based on the kinetic data.

procedures are shown in the Supplemental Data). We used the initial rate of inactivation (0–10 min) showing pseudo first-order kinetics to determine the inhibition constants. The enzyme activity is, however, not reduced to zero over the time period, perhaps because of the decomposition of the thioester intermediate or the existence of two populations of the enzymes. As shown in Table 1, benzotriazole esters **3–10** are strong inhibitors, and, among these, **8** is the most potent, with an inactivation constant of 1.1 × 10^{-3} s^{-1} and an inhibition constant of 7.5 nM. In addition, these esters are not toxic to Vero E6 cells, which are often used in the cell-based assay for SARS-CoV [14], at a concentration of 100 μM. Compound **8** represents the most potent mechanism-based 3CL^{pro} inhibitor reported to date.

We also investigated the nature of the inhibited enzyme by mass spectrometry. Electrospray ionization mass spectra of wild-type 3CL^{pro} and 3CL^{pro} treated with 4-(dimethylamino)benzoyl ester **4** (2 hr of incubation and 18 hr of dialysis) and their deconvoluted mass spectra were determined (see the Supplemental Data). The mass difference of 148.6 Da between the peaks of 33847.35 ($[M + H]^+$) and 33995.93 ($[M + H]^+$) implies the acylation of 3CL^{pro} with a 4-(dimethylamino)benzoyl moiety (mass 147.12). To further investigate the acylation site, MALDI-TOF mass spectrometric analysis of the trypsin digest of 3CL^{pro} and 3CL^{pro} treated with 4-(dimethylamino)benzoyl ester **4** was performed. From the MALDI spectra of the tryptic 3CL^{pro} and the tryptic acylated 3CL^{pro} of G138-K180 peptide fragments, a mass shift of 147 Da between T15 (4594.11 Da) and acylated T15 (4741.31 Da) indicates that this peptide fragment contains an acylated residue (Figures 3A and 3B). In order to determine the acylation site on the acylated T15 peptide, we performed a sequence analysis by MALDI MS/MS for peptides T15 and acylated T15 as depicted in Figure 3C. There is no mass difference among y series fragment ions up to y_{27}, but a mass shift of 147.2 Da (4149.6 Da versus 4296.8 Da) on b_{39} clearly shows that Cys145 is the only acylation site. This is consistent with the observation of no mass shift of mutant C145A 3CL^{pro} treated with 4-(dimethylamino)benzoyl ester **4**. All of these results support the mechanism of irreversible inhibition of 3CL^{pro} by 4-(dimethylamino)benzoyl ester **4** via acylation of Cys145 (Figure 4).

In order to develop stable, noncovalent inhibitors based on the benzotriazole esters discovered in this study, we synthesized compounds **13** and **14** by using TBAF-assisted N-alkylation of 1*H*-benzotriazole **11** [28, 29]. In addition, compound **13** was hydrogenated with $Pd(OH)_2$/C as a catalyst at room temperature to obtain compounds **15** (82%) and **16** (13%). Compounds **15** and **16** were methylated or dimethylated to compounds **17–20** by using TBAF as a reagent (Figure 5A). Compounds **13–20** have all the features of benzotriazole ester inhibitors, except that the ester oxygen is replaced by a carbon. Inhibition analysis shows that compounds **13–20** are noncovalent competitive inhibitors, albeit relatively weak ones compared to the corresponding esters; of these, compound **14** is most potent, with a K_i of 1.0 μM. Reduction of the carbonyl group, however, results in a significant loss of activity (Figure 5A). It is noted that the benzotriazole compounds contain three equilibrium structures in solution (Figure 5B) [25, 26], and that compounds **13–20** may mimic the ester forms instead of the three equilibrium forms found in solution.

To gain further insight into the mode of inhibition, a docking experiment based on computer modeling (Autodock version 3.0.5) [30] for the binding of compounds **3**, **4**, **8**, and **9** with 3CL^{pro} (1uk4) [12] was carried out, and the result indicated that the benzotriazole moiety was disposed in the pocket formed by Cys145, Ser144, and Gly143 in the active site (Figure 6). The γ-S atom of Cys145 was close enough, within 3.5 Å in a rigid model, to the carbonyl group of the benzotriazole ester to render a nucleophilic attack. The aminophenyl group (for **3** and **4**) and the indole moiety (for **8** and **9**) were in the region surrounded by Thr25, Thr26, His41, Thr45, Ala46, and Met49. The NH group of the indole moiety of **8** was hydrogen bonded with the side chain OH of Thr25. In comparison, the indole group of **9** lacks such hydrogen bonding and thus shows a weaker affinity

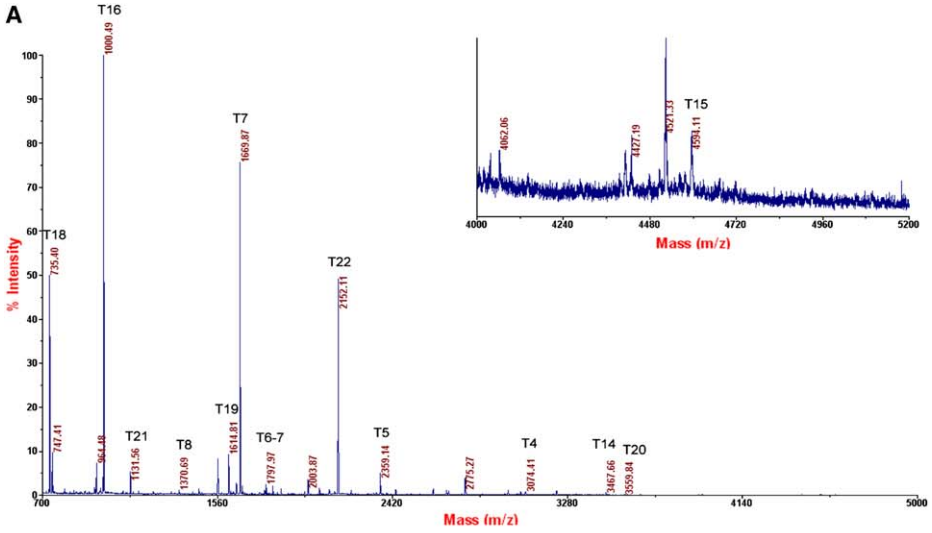
A
T16
1000.49
T7
1669.87
T18
735.40
T22
2152.11
T19
1614.81
T21
1131.56
T8
1370.69
T6-7
1797.97
T5
2359.14
T4
3074.41
T14
3467.66
T20
3559.84
T15
4062.06
4427.19
4521.33
4594.11
% Intensity
Mass (m/z)

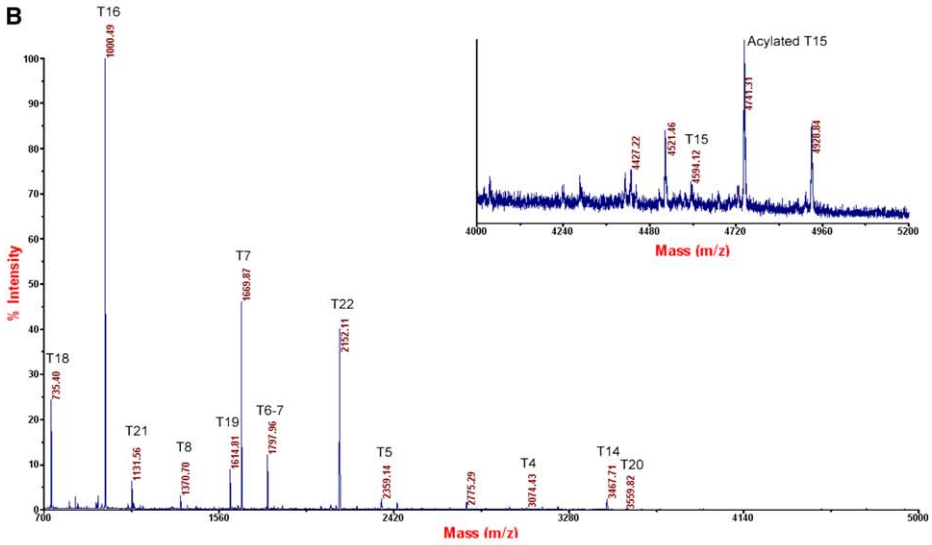
B
T16
1000.49
Acylated T15
4741.31
4528.34
T15
4427.22
4521.46
4594.12
T7
1669.87
T22
2152.11
T18
735.40
T21
1131.56
T19
1614.81
T6-7
1797.96
T8
1370.70
T5
2359.14
T4
3074.43
T14
3467.71
T20
3559.82
% Intensity
Mass (m/z)

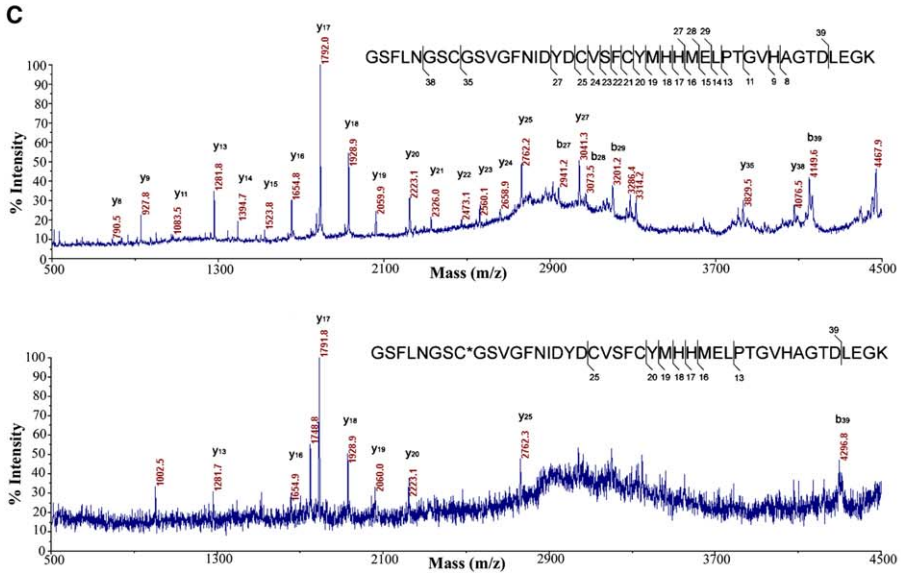
C
GSFLNGSCGSVGFNIDYDCVSFCYMHHMELPTGVHAGTDLEGK
GSFLNGSC*GSVGFNIDYDCVSFCYMHHMELPTGVHAGTDLEGK
% Intensity
Mass (m/z)

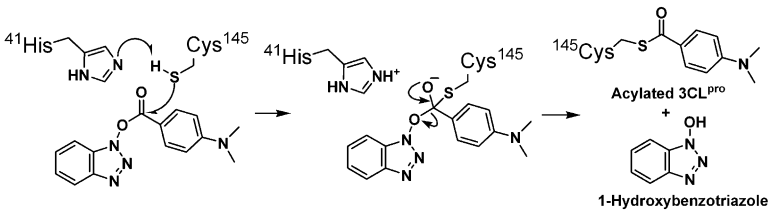

Figure 4. Proposed Mechanism for Inhibition of SARS-CoV 3CL^{pro} by Acylation with Benzotriazole Esters

toward 3CL^{pro} than does isomer **8**. Compounds **13–20** do not fit into the pocket well enough to interact with the residues mentioned above, and the calculated minimal energies of binding are ~0.5–1.0 kcal/mol higher than those of the corresponding esters, consistent with the inhibition assay result (see the Supplemental Data).

Significance

Severe acute respiratory syndrome (SARS) is a newly emerged disease caused by a novel human coronavirus. Currently, no effective antiviral agents exist against this deadly epidemic. The main protease of SARS-CoV, 3CL^{pro}, is an attractive target for drug discovery due to its essential role in viral replication. We have discovered several stable benzotriazole esters as a new class of irreversible enzyme inhibitors, and, to our knowledge, these compounds are the most potent mechanism-based 3CL^{pro} inhibitors known to date. The mode of action has been studied and has been shown to proceed through acylation of the active site Cys145 assisted by the catalytic dyad.

Experimental Procedures

Materials and Methods

SARS-CoV 3CL protease was prepared according to the previously described procedure [31]. Reactions requiring dry conditions were carried out under an inert atmosphere by using standard techniques. All of the reagents and solvents were reagent grade and were used without further purification unless otherwise specified. THF was distilled from sodium benzophenone ketyl under N_2. HRMS values were obtained by using the EI as the ionization source.

General Procedure for the Preparation of Benzotriazole Esters

To a solution of acid compound (1.0 equiv.), 2-(1*H*-benzotriazole-1-yl)-1,1,3,3-tetramethyluronium hexafluorophosphate (HBTU, 1.1 equiv) in DMF (1.0 ml), as well as *N*,*N*-diisopropylethylamine (DIEA, 1.1 equiv.), was added. After the solution was stirred at 25ºC for 3.0 hr, the reaction mixture was added to 1 M $NaHCO_3$ (10 ml) and extracted with ethyl acetate (EA) (15 ml × 3), and the organic layer was collected and concentrated under reduced pressure. The residue was purified by use of column chromatography on silica gel to provide the desired 1-hydroxybenzotriazole esters.

2-Aminobenzoic Acid Benzotriazol-1-yl Ester, 3

The standard procedure was followed by use of 2-aminobenzoic acid (**C9**, 34.8 mg, 0.2537 mmol, 1.0 equiv.), HBTU (105.9 mg, 0.2791 mmol, 1.1 equiv.), and DIEA (49 μl, 0.2791 mmol, 1.1 equiv.). After the reaction mixture was worked up, the residue was purified by use of column chromatography (5% MeOH in chloroform as eluant). Benzotriazole ester **3** (57.4 mg, 0.2258 mmol) was obtained in 89% yield as a yellow solid: TLC R_f = 0.81 (5% MeOH in $CHCl_3$ as eluant); ^{1}H NMR ($CDCl_3$, 400 MHz) δ = 5.31 (brs, 2 H, NH_2), 6.73–6.78 (m, 2 H, 2 × ArH), 7.41 (t, 2 H, *J* = 6.0 Hz, 2 × ArH), 7.46 (d, 1 H, *J* = 6.6 Hz, ArH), 7.52 (t, 1 H, *J* = 6.0 Hz, ArH), 8.06 (d, 2 H, *J* = 6.7 Hz, ArH), 8.14 (d, 1 H, *J* = 6.7 Hz, ArH); ^{13}C NMR ($CDCl_3$, 100 MHz) δ = 104.26, 108.45, 116.82, 116.98, 120.42, 124.78, 128.66, 129.00, 130.84, 136.71, 143.50, 152.23, 163.65; IR (KBr) 3456 (m, NH), 3322 (m, NH), 1736 (s, C=O), 1632 (s), 1566 (m), 1485 (s), 1372 (m), 1228 (s), 1153 (s), 977 (s), 740 (s) cm^{-1}; HRMS [M + 1] calcd for $C_{13}H_{11}N_4O_2$: 255.0875, found 255.0882.

4-Dimethylamino-Benzoic Acid Benzotriazol-1-yl Ester, 4

The standard procedure was followed by use of (dimethylamino)-benzoic acid (**D6**, 120.3 mg, 0.7283 mmol, 1.0 equiv.), HBTU (303.8 mg, 0.8011 mmol, 1.1 equiv.), and DIEA (140 μl, 0.8011 mmol, 1.1 equiv.). After the reaction mixture was worked up, the residue was purified by use of column chromatography (chloroform as eluant). Benzotriazole ester **4** (191.2 mg, 0.6773 mmol) was obtained in 93% yield as a light-yellow solid: TLC R_f = 0.50 ($CHCl_3$ as eluant); ^{1}H NMR ($CDCl_3$, 400 MHz) δ = 3.13 (s, 6 H, 2 × CH_3), 6.74 (d, *J* = 8.9 Hz, 2 H, 2 × ArH), 7.42 (t, *J* = 6.7 Hz, 1 H, ArH), 7.47–7.55 (m, 2 H, 2 × ArH), 8.07–8.12 (m, 3 H, 3 × ArH); ^{13}C NMR ($CDCl_3$, 100 MHz) δ = 40.01, 108.64, 110.02, 111.06, 120.35, 124.54, 128.36, 129.11, 132.73, 143.57, 154.38, 163.51; IR (KBr) 2914 (w), 1768 (s, C=O), 1609 (s), 1537 (s), 1441 (s), 1386 (s), 1263 (s), 1183 (s), 957 (s), 770 (s) cm^{-1}; HRMS [M + 1] calcd for $C_{15}H_{15}N_4O_2$: 283.1195, found 283.1199.

4-Methylamino-Benzoic Acid Benzotriazol-1-yl Ester, 5

The standard procedure was followed by use of (4-methylamino)-benzoic acid (**D5**, 53.5 mg, 0.3539 mmol, 1.0 equiv.), HBTU (147.7 mg, 0.3894 mmol, 1.1 equiv.), and DIEA (68 μl, 0.3894 mmol, 1.1 equiv.). After the reaction mixture was worked up, the residue was purified by use of column chromatography (chloroform as eluant). Benzotriazole ester **5** (88.3 mg, 0.3291 mmol) was obtained in 93% yield as a white solid: TLC R_f = 0.28 ($CHCl_3$ as eluant); ^{1}H NMR ($CDCl_3$, 400 MHz) δ = 2.92 (d, 3 H, *J* = 1.5 Hz, CH_3N), 6.63 (d, 2 H, *J* = 8.7 Hz, 2 × ArH), 7.41 (t, 1 H, *J* = 7.6 Hz, ArH), 7.46–7.53 (m, 2 H, 2 × ArH), 8.04–8.07 (m, 3 H, 3 × ArH); ^{13}C NMR ($CDCl_3$, 100 MHz) δ = 29.91, 108.61, 111.05, 111.52, 120.29, 124.62, 128.43, 129.05, 133.00, 143.52, 154.70, 162.70; IR (KBr) 3346 (m, NH), 3010 (m), 2907 (w), 1764 (s, C=O), 1602 (s), 1545 (s), 1497 (s), 1446 (s), 1362 (s), 1238 (s), 1068 (s), 957 (s), 791 (s) cm^{-1}; HRMS [M + 1] calcd for $C_{14}H_{13}N_4O_2$: 269.1039, found 269.1032.

4-Diethylamino-Benzoic Acid Benzotriazol-1-yl Ester, 6

The standard procedure was followed by use of (diethylamino)benzoic acid (**D7**, 48.4 mg, 0.2505 mmol, 1.0 equiv.), HBTU (104.5 mg, 0.2755 mmol, 1.1 equiv.), and DIEA (48 μl, 0.2755 mmol, 1.1 equiv.). After the reaction mixture was worked up, the residue was purified by use of column chromatography (chloroform as eluant). Benzotriazole ester **6** (71.5 mg, 0.2304 mmol) was obtained in 92% yield as a light-yellow solid: TLC R_f = 0.50 ($CHCl_3$ as eluant); ^{1}H NMR ($CDCl_3$, 400 MHz) δ = 1.17–1.25 (m, 6 H, 2 × CH_3), 3.38–3.49 (m, 4 H, 2 × CH_2), 6.70 (d, 2 H, *J* = 8.8 Hz, 2 × ArH), 7.40 (t, *J* = 7.4 Hz,

Figure 3. MALDI Spectrum of Inhibitor **4** and SARS 3CL^{pro}

(A) MALDI spectrum of tryptic 3CL^{pro}.

(B) MALDI spectrum of tryptic acylated 3CL^{pro}.

(C) MALDI MS/MS spectra of T15 and acylated T15 peptides (GSFLNGSC*GSVGFNIDYDCVSFCYMHHMELPTGVHAGTDLEGK) showed a mass shift of 147.2 Da (4149.6 Da versus 4296.8 Da) on b_{39}, indicating that Cys145 (C*) is the acylation site.

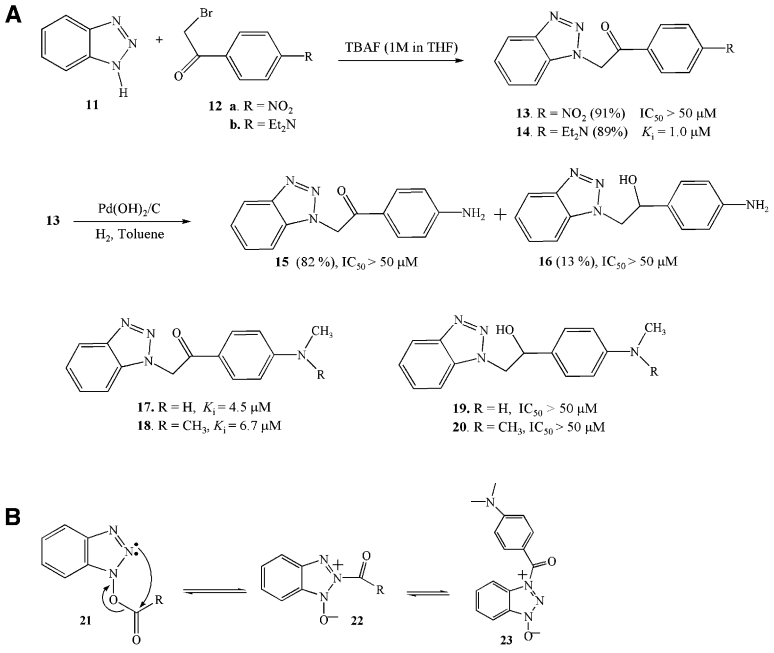

Figure 5. Synthesis of Noncovalent Inhibitors

(A) Synthesis of compounds **13–20** and their IC_{50}s or K_is for SARS-CoV $3CL^{pro}$.

(B) The equilibrium structures of the benzotriazole compounds in solution.

1 H, ArH), 7.42–7.53 (m, 2 H, 2 × ArH), 6.70 (d, 1 H, *J* = 8.8 Hz, ArH), 8.06 (d, *J* = 8.8 Hz, 2 H, 2 × ArH); ^{13}C NMR ($CDCl_3$, 100 MHz) δ = 12.39, 44.66, 108.63, 110.64, 120.29, 124.53, 128.33, 128.89, 132.23, 133.01, 143.53, 152.61, 162.69; IR (KBr) 2980 (m), 1774 (s, C=O), 1602 (s), 1529 (s), 1445 (s), 1380 (s), 1260 (s), 1155 (s), 963 (s), 766 (s) cm^{-1}; HRMS [M + 1] calcd for $C_{17}H_{19}N_4O_2$: 311.1508, found 311.1503.

1*H*-Benzoimidazole-5-Carboxylic Acid Benzotriazol-1-yl Ester, 7

The standard procedure was followed by use of 5-benzimidazole-carboxylic acid (**G5**, 39.1 mg, 0.2411 mmol, 1.0 equiv.), HBTU (100.6 mg, 0.2652 mmol, 1.1 equiv.), and DIEA (46 μl, 0.2652 mmol, 1.1 equiv.). After the reaction mixture was worked up, the residue was purified by use of column chromatography (chloroform as eluant). Benzotriazole ester **7** (48.5 mg, 0.1737 mmol) was obtained in 72% yield as a light-brown solid: TLC R_f = 0.21 (10% MeOH in $CHCl_3$ as eluant); ^{1}H NMR (d_4-methanol + $CDCl_3$, 400 MHz) δ = 7.47–7.53 (m, 2 H, 2 × ArH), 7.79–7.84 (m, 2 H, 2 × ArH), 8.04 (d, 1 H, *J* = 8.5 Hz, ArH), 8.17 (dd, 1 H, *J* = 8.5, 1.6 Hz, ArH), 8.49 (s, 1 H, N=CH), 8.61 (d, 1 H, *J* = 1.6 Hz, ArH); ^{13}C NMR (d_4-methanol + $CDCl_3$, 100 MHz) δ = 108.53, 110.19, 115.19, 117.00, 118.35, 119.38, 124.66, 125.11, 125.96, 126.82, 128.88, 143.11, 144.83, 163.12; IR (KBr) 3099 (m, NH), 2901 (w), 1778 (s, C=O), 1620 (s), 1576 (m), 1421 (s), 1362 (s), 1281 (s), 1155 (s), 993 (s), 739 (s) cm^{-1}; HRMS [M + 1] calcd for $C_{14}H_{10}N_5O_2$: 280.0834, found 280.0834.

1*H*-Indole-5-Carboxylic Acid Benzotriazol-1-yl Ester, 8

The standard procedure was followed by use of indole-5-carboxylic acid (70.6 mg, 0.4381 mmol, 1.0 equiv.), HBTU (182.8 mg, 0.4819 mmol, 1.1 equiv.), and DIEA (84 μl, 0.4819 mmol, 1.1 equiv.). After the reaction mixture was worked up, the residue was purified by use of column chromatography (chloroform as eluant). Benzotriazole ester **8** (107.3 mg, 0.3855 mmol) was obtained in 88% yield as a brown solid: ^{1}H NMR (d_6-acetone, 400 MHz) δ = 6.78 (d, 1 H, *J* = 3.08 Hz,), 7.52 (t, 1 H, *J* = 7.1 Hz, ArH), 7.59 (t, 1 H, *J* = 2.3 Hz, ArH),

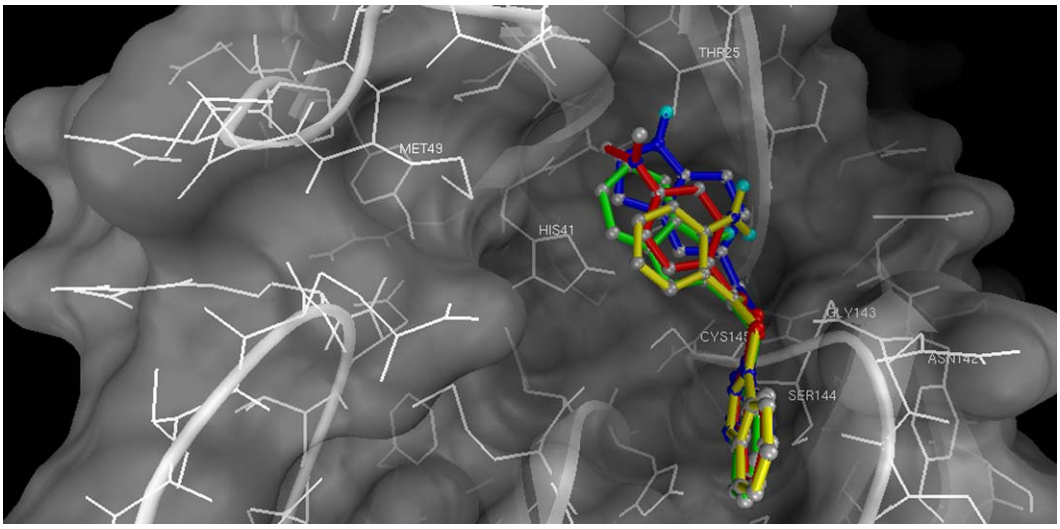

Figure 6. A Modeling Complex of SARS $3CL^{pro}$ and Benzotriazole Esters

Binding modes of compounds **3** (yellow), **4** (red), **8** (blue), and **9** (green) in the active site of SARS-CoV $3CL^{pro}$ (PDB luk4). Models were generated by Autodock and displayed by MGLTOOLS (MGL, Scripps).

7.65 (t, 1 H, *J* = 8.4 Hz, ArH), 7.68 (d, 1 H, *J* = 8.6 Hz, =CH), 7.79 (d, 1 H, *J* = 8.4 Hz, ArH), 8.01 (d, 1 H, *J* = 8.4 Hz, ArH), 8.10 (d, 1 H, *J* = 8.6 Hz, =CH), 8.68 (s, 1 H, ArH); ^{13}C NMR (d_6-acetone, 100 MHz) δ = 104.06, 109.58, 112.82, 115.65, 120.64, 123.78, 125.56, 125.79, 128.53, 128.90, 129.50, 129.78, 141.00, 144.27, 164.87; IR (KBr) 3213 (m, NH), 2907 (w), 1767 (s, C=O), 1614 (s), 1582 (m), 1446 (s), 1359 (s), 1266 (s), 1157 (s), 990 (s), 789 (s) cm^{-1}; HRMS [M + 1] calcd for $C_{15}H_{11}N_4O_2$: 279.0882, found 279.0878.

1*H*-Indole-2-Carboxylic Acid Benzotriazol-1-yl Ester, 9

The standard procedure was followed by use of indole-2-carboxylic acid (**F1**, 74.9 mg, 0.4648 mmol, 1.0 equiv.), HBTU (193.9 mg, 0.5113 mmol, 1.1 equiv.), and DIEA (89 μl, 0.5113 mmol, 1.1 equiv.). After the reaction mixture was worked up, the residue was purified by use of column chromatography (chloroform as eluant). Benzotriazole ester **9** (115.1 mg, 0.4136 mmol) was obtained in 89% yield as a light-yellow solid: TLC R_f = 0.82 (5% MeOH in $CHCl_3$ as eluant); ^{1}H NMR ($CDCl_3$, 400 MHz) δ = 7.24 (t, 1 H, *J* = 8.0 Hz, ArH), 7.41–7.46 (m, 2 H, 2 × ArH), 7.49–7.58 (m, 3 H, 3 × ArH), 7.69 (s, 1 H, =CH), 7.78 (d, 1 H, *J* = 8.2 Hz, ArH), 8.10 (1 H, *J* = 8.4 Hz, ArH), 9.97 (br, 1 H, NH); ^{13}C NMR ($CDCl_3$, 100 MHz) δ = 38.58, 108.37, 112.48, 113.28, 120.45, 120.69, 121.69, 123.11, 124.90, 127.06, 127.29, 128.83, 138.60, 143.42, 157.99; IR (KBr) 3282 (m, NH), 1773 (s, C=O), 1670 (s), 1517 (s), 1459 (s), 1389 (s), 1340 (s), 1161 (s), 1052 (s), 778 (s) cm^{-1}; HRMS [M + 1] calcd for $C_{15}H_{11}N_4O_2$: 279.0882, found 279.0878.

1*H*-Benzoimidazole-5-Carboxylic Acid Benzotriazol-1-yl Ester, 10

The standard procedure was followed by use of 5-fluoroindole-2-carboxylic acid (**F4**, 26.1 mg, 0.1457 mmol, 1.0 equiv.), HBTU (60.8 mg, 0.1603 mmol, 1.1 equiv.), and DIEA (28 μl, 0.1603 mmol, 1.1 equiv.). After the reaction mixture was worked up, the residue was purified by use of column chromatography (chloroform as eluant). Benzotriazole ester **10** (39.3 mg, 0.1327 mmol) was obtained in 91% yield as a light-yellow solid: TLC R_f = 0.83 (5% MeOH in $CHCl_3$ as eluant); ^{1}H NMR (d_6-DMSO and $CDCl_3$, 400 MHz) δ = 7.15 (dd, 1 H, *J* = 7.4, 2.4 Hz, ArH), 7.41–7.52 (m, 3 H, 3 × ArH), 7.58–7.65 (m, 2 H, ArH + =CH), 7.71 (d, 1 H, *J* = 8.4 Hz, ArH), 8.07 (1 H, *J* = 8.4 Hz, ArH); ^{13}C NMR (d_6-DMSO and $CDCl_3$, 100 MHz) δ = 106.15 (d, *J* = 24.0 Hz), 108.60, 111.92 (d, *J* = 6.0 Hz), 114.14 (d, *J* = 10.0 Hz), 115.61 (d, *J* = 27.0 Hz), 119.66, 121.80, 124.79, 126.35 (d, *J* = 11.0 Hz), 128.26, 128.77, 135.58, 142.65, 156.32 (d, *J* = 235.0 Hz), 157.34; IR (KBr) 3231 (m, NH), 2981 (w), 1782 (s, C=O), 1681 (s), 1521 (m), 1434 (s), 1342 (s), 1222 (s), 1186 (s), 921 (s), 757 (s) cm^{-1}; HRMS [M + 1] calcd for $C_{15}H_{10}FN_4O_2$: 297.0779, found 297.0788.

General Procedure for the TBAF-Assisted Benzotriazole N-Alkylation, 14

Benzotriazole (100 mg, 0.84 mmol) and α-bromo-4-(diethylamino) acetophenone (272 mg, 1.00 mmol, 1.2 equiv.) were placed in a 5 ml flask with a stirring bar, followed by the addition of TBAF (1.00 ml, 0.84 mmol, 1.2 equiv., 1 M in THF) at room temperature. After being stirred for 2 hr at room temperature, the reaction was directly loaded into the column, and the product was eluted with a solution of 6:1 hexane:ethyl acetate to yield 217.4 mg (84%) of product as a pale-yellow solid. ^{1}H NMR (500 MHz, $CDCl_3$) δ 8.05 (d, *J* = 8.5 Hz, 1 H), 7.96 (d, *J* = 9.2 Hz, 2 H), 7.50–7.30 (m, 3 H), 6.68 (d, *J* = 9.2 Hz, 2 H), 5.98 (s, 2 H), 3.42 (q, *J* = 7.0 Hz, 4 H), 1.19 (t, *J* = 7.0 Hz, 6 H); ^{13}C NMR (125 MHz, $CDCl_3$) δ 187.92, 152.46, 146.42, 134.38, 131.37, 128.00, 124.21, 121.41, 120.25, 110.91, 110.46, 53.76, 45.06, 12.87; ESI-MS calculated for $C_{18}H_{20}N_4O$ 308.16, found 308.12.

Inhibition Assay against the SARS-CoV 3CL Protease

A fluorometric assay [31] was utilized to determine the inhibition constants of the prepared samples. Briefly, a fluorogenic peptide, Dabcyl-KTSAVLQSGFRKME-Edans, was used as the substrate [31], and the enhanced fluorescence due to cleavage of this substrate catalyzed by the protease was monitored at 538 nm with excitation at 355 nm. The IC_{50} value of individual inhibitors was measured in a reaction mixture containing 50 nM SARS 3CL protease and 6 μM fluorogenic substrate in 20 mM Bis-Tris (pH 7.0). The enzyme stock solution was kept in 12 mM Tris-HCl (pH 7.5) containing 120 mM NaCl, 0.1 mM EDTA, plus 7.5 mM β-ME before being added to the assay solution. The K_i measurements (for the noncovalent inhibitors case) were performed at two fixed inhibitor concentrations and various substrate concentrations. In the mechanism-based inactivator cases, we used $t_{1/2}$ versus 1/[inactivator] for Ki measurements (for more detailed procedures for the behavior of inhibitors, please see the Supplemental Data).

Expression and Purification of SARS-CoV 3CL^{pro}

Wild-type and the C145A mutant of the SARS protease were cloned in pET 28 with N-terminal Trx, His tag, and FXa site. The tags were removed by FXa protease after the proteins were purified with NiNTA column chromatography. For more detailed experimental procedures, please see [32].

Mass Spectrometric Analysis

The ESI-MS experiments were conducted on a Bruker Daltonics BioTOF III high-resolution mass spectrometer, equipped with a home-built nanoESI source. Mass resolution was better than 20,000 on one-pass mode with a mass range of ~100–3,000. The samples were diluted to 1.0 μM with bidistilled aqueous solution containing 40% methanol and 0.1% formic acid (v/v/v) and were infused with a syringe pump at a flow rate of 300 nl/min. The actual amount of samples consumed was less than 300 fmole.

The MALDI-MS measurements were performed on a MALDI-TOF/TOF mass spectrometer (Applied Biosystems 4700 Proteomics Analyzer). Tryptic digest solution was mixed 1:1 with matrix solution (CHCA [α-cyano-4-hydroxycinnamic acid] 10 mg/ml in solvents 49.9/50/0.1 $H_2O/CH_3CN/TFA$), and 1.0 μl was then spotted in each well. Each MALDI spectrum was accumulated from up to 4,000 laser shots from a random sampling of 40 positions per well.

Computer Modeling of SARS-CoV 3CL Protease Inhibition

Docking was performed by using Autodock, version 3.05 [30]. Precomputed energy grid maps with grid point spacing of 0.375 Å and 50 × 50 × 50 grid points centered at the active site were used (autogrid tool in Autodock, version 3.05). During a docking experiment, each compound was kept flexible (except their rings and amide bonds), and the built-in LGA method was adopted. In each compound structure, 1.5 × 10^6 energy was evaluated, and 40 poses were selected from 2.7 × 10^5 generations per run.

The crystal structure of SARS-CoV 3CL protease in complex with a substrate-analog inhibitor (coded 1uk4) was obtained from The Protein Data Bank (PDB; http://www.rcsb.org/pdb/) (for more detailed procedures, please see the Supplemental Data).

Supplemental Data

Supplemental data including 90 different acids, the X-ray data for compound **4**, synthesis and characterization of compounds **15–20**, a supplemental enzyme kinetic study, and the detailed molecular docking data are available at http://www.chembiol.com/cgi/content/full/13/3/261/DC1/.

Acknowledgments

This work is supported by the National Science Council, Taiwan and Genomics Research Center, Academia Sinica. We also thank Ms. Hsien-Hua Hsu for her help with the cytotoxicity assay.

Received: July 12, 2005
Revised: December 16, 2005
Accepted: December 27, 2005
Published online: March 24, 2006

References

1. Ksiazek, T.G., Erdman, D., Goldsmith, C.S., Zaki, S.R., Peret, T., Emery, S., Tong, S., Urbani, C., Comer, J.A., Lim, W., et al. (2003). A novel coronavirus associated with severe acute respiratory syndrome. N. Engl. J. Med. *348*, 1953–1966.
2. Drosten, C., Günther, S., Preiser, W., van der Werf, S., Brodt, H.-R., Becker, S., Rabenau, H., Panning, M., Kolesnikova, L., Fouchier, R.A.M., et al. (2003). Identification of a novel

coronavirus in patients with severe acute respiratory syndrome. N. Engl. J. Med. *348*, 1967–1976.

3. Peiris, J.S.M., Lai, S.T., Poon, L.L.M., Guan, Y., Yam, L.Y.C., Lim, W., Nicholls, J., Yee, W.K.S., Yan, W.W., Cheung, M.T., et al. (2003). Coronavirus as a possible cause of severe acute respiratory syndrome. Lancet *361*, 1319–1325.
4. Lee, N., Hui, D., Wu, A., Chan, P., Cameron, P., Joynt, G.M., Ahuja, A., Yung, M.Y., Leung, C.B., To, K.F., et al. (2003). A major outbreak of severe acute respiration syndrome in Hong Kong. N. Engl. J. Med. *348*, 1986–1994.
5. Poutanen, S.M., Low, D.E., Henry, B., Finkelstein, S., Rose, D., Green, K., Tellier, R., Draker, R., Adachi, D., Ayers, M.N., et al. (2003). Canadian severe acute respiratory syndrome study, identification of severe acute respiratory syndrome in Canada. N. Engl. J. Med. *348*, 1995–2005.
6. Tsang, K.W., Ho, P.L., Ooi, G.C., Yee, W.K., Wang, T., Chan-Yeung, M., Lam, W.K., Seto, W.H., Yam, L.Y., Cheung, T.M., et al. (2003). A cluster of cases of severe acute respiratory syndrome in Hong Kong. N. Engl. J. Med. *348*, 1977–1985.
7. He, J.-F., Peng, G.-W., Min, J., Yu, D.-W., Liang, W.-J., Zhang, S.-Y., Xu, R.-H., Zheng, H.-Y., Wu, X.-W., Xu, J., et al. (2004). Molecular evolution of the SARS coronavirus during the course of the SARS epidemic in China. Science *303*, 1666–1669.
8. Rota, P.A., Oberste, M.S., Monroe, S.S., Nix, W.A., Campagnoli, R., Icenogle, J.P., Penaranda, S., Bankamp, B., Maher, K., Chen, M.-H., et al. (2003). Characterization of a novel coronavirus associated with severe acute respiratory syndrome. Science *300*, 1394–1399.
9. Marra, M.A., Jones, S.J.M., Astell, C.R., Holt, R.A., Brooks-Wilson, A., Butterfield, Y.S.N., Khattra, J., Asano, J.K., Barber, S.A., Chan, S.Y., et al. (2003). The genome sequence of the SARS-associate coronovirus. Science *300*, 1399–1404.
10. Ruan, Y., Wei, C.L., Lin, A.E., Vega, V.B., Thoreau, H., Se-Thoe, S.Y., Chia, J.M., Ng, P., Chiu, K.P., Lim, L., et al. (2003). Comparative full-length genome sequence analysis of 14 SARS coronovirus isolates and common mutations associated with putative origins of infection. Lancet *361*, 1779–1785.
11. Anand, K., Ziebuhr, J., Wadhwani, P., Mesters, J.R., and Hilgenfeld, R. (2003). Coronavirus main protease ($3CL^{pro}$) structure: basis for design of anti-SARS drugs. Science *300*, 1763–1767.
12. Yang, H., Yang, M., Ding, Y., Liu, Y., Lou, Z., Zhou, Z., Sun, L., Mo, L., Ye, S., Pang, H., et al. (2003). The crystal structure of severe acute respiratory syndrome virus main protease and its complex with an inhibitor. Proc. Natl. Acad. Sci. U.S.A. *100*, 13190–13195.
13. Chou, K., Wei, D., and Zhong, W. (2003). Binding mechanism of coronavirus main protease with ligands and its implication to drug design against SARS. Biochem. Biophys. Res. Commun. *308*, 148–151.
14. Wu, C.-Y., Jan, J.-T., Ma, H.-H., Kuo, C.-J., Juan, H.-F., Cheng, Y.-S.E., Hsu, H.-H., Huang, H.-C., Wu, D., Brik, A., et al. (2004). Small molecules targeting severe acute respiratory syndrome human coronavirus. Proc. Natl. Acad. Sci. USA *101*, 10012–10017.
15. Hsu, J.T.-A., Kuo, C.-J., Hsieh, H.-P., Wang, Y.-C., Huang, K.-K., Lina, C.P.-C., Huang, P.-F., Chen, X., and Liang, P.-H. (2004). Evaluation of metal-conjugated compounds as inhibitors of 3CL protease of SARS-CoV. FEBS Lett. *574*, 116–120.
16. Bacha, U., Barrila, J., Velazquez-Campoy, A., Leavitt, S.A., and Freire, E. (2004). Identification of novel inhibitors of the SARS coronavirus main protease $3CL^{pro}$. Biochemistry *43*, 4906–4912.
17. Kao, R.Y., Tsui, W.H.W., Lee, T.S.W., Tanner, J.A., Watt, R.M., Huang, J.-D., Hu, L., Chen, G., Chen, Z., Zhang, L., et al. (2004). Identification of novel small-molecular inhibitors of severe acute respiratory syndrome-associated coronavirus by chemical genetics. Chem. Biol. *11*, 1293–1299.
18. Blanchard, J.E., Elowe, N.H., Huitema, C., Fortin, P.D., Cechetto, J.D., Eltis, L.D., and Brown, E.D. (2004). High-throughput screening identifies inhibitors of the SARS coronavirus main proteinase. Chem. Biol. *11*, 1445–1453.
19. Jain, R.P., Pettersson, H.I., Zhang, J., Aull, K.D., Fortin, P.D., Huitema, C., Eltis, L.D., Parrish, J.C., James, M.N.G., Wishart, D.S., et al. (2004). Synthesis and evaluation of keto-glutamine analogues as potent inhibitors of severe acute respiratory syndrome $3CL^{pro}$. J. Med. Chem. *47*, 6113–6116.
20. Shie, J.-J., Fang, J.-M., Kuo, C.-J., Kuo, T.-H., Liang, P.-H., Huang, H.-J., Yang, W.-B., Lin, C.-H., Chen, J.-L., Wu, Y.-T., et al. (2005). Discovery of potent anilide inhibitors against the severe acute respiratory syndrome 3CL protease. J. Med. Chem. *48*, 4469–4473.
21. Brik, A., Lin, Y.-C., Elder, J., and Wong, C.-H. (2002). A quick diversity-oriented amide-forming reaction to optimize p-subsite residues of HIV protease inhibitors. Chem. Biol. *9*, 891–896.
22. Wu, C.-Y., Chang, C.-F., Chen, J.S.-Y., Wong, C.-H., and Lin, C.-H. (2003). Rapid diversity-oriented synthesis in microtiter plates for in situ screening: discovery of potent and selective α-fucosidase inhibitors. Angew. Chem. Int. Ed. *42*, 4661–4664.
23. Chang, C.-F., Ho, C.-W., Wu, C.-Y., Chao, T.-A., Wong, C.-H., and Lin, C.-H. (2004). Discovery of picomolar slow tight-binding inhibitors of α-fucosidase. Chem. Biol. *11*, 1301–1306.
24. Stoner, E.J., Cooper, A.J., Dickman, D.A., Kolaczkowski, L., Lallaman, J.E., Liu, J.-H., Oliver-Shaffer, P.A., Patel, K.M., Paterson, J.B., Jr., Plata, D.J., et al. (2000). Synthesis of HIV protease inhibitor ABT-378 (Lopinavir). Org. Proc. Res. Dev. *4*, 264–269.
25. McCarthy, D.G., Hegarty, A.F., and Hathaway, B.J. (1977). N-hydroxy-compounds as acyl transfer agents. Part 1. kinetics and mechanism of nucleophilic displacements on 1-hydroxybenzotriazole esters and crystal and molecular structure of 1-benzoyloxybenzotriazole. J. Chem. Soc. Perkin II *2*, 224–231.
26. Barlos, K., Papaioannou, D., and Voliotis, S. (1985). Crystal structure of 3-(N^{α}-tritylmethionyl)-benzotriazole 1-oxide, a synthon in peptide synthesis. J. Org. Chem. *50*, 696–697.
27. Hansh, C., Leo, A., and Taft, R.W. (1991). A survey of Hammett substituent constants and resonance and field parameters. Chem. Rev. *91*, 165–195.
28. Brik, A., Wu, C.-Y., Best, M.D., and Wong, C.-H. (2005). Tetrabutylammonium fluoride-assisted rapid N9-alkylation on purine ring: application to combinatorial reactions in microtiter plates for the discovery of potent sulfotransferase inhibitors in situ. Bioorg. Med. Chem. *13*, 4622–4626.
29. Wu, C.-Y., Brik, A., Wang, S.-K., Chen, Y.-S., and Wong, C.-H. (2005). Tetrabutylammonium fluoride-mediated rapid alkylation reaction in microtiter plates for discovery of enzyme inhibitors in situ. Chembiochem. *6*, 2176–2180.
30. Morris, G.M., Goodsell, D.S., Halliday, R.S., Huey, R., Hart, W.E., Belew, R.K., and Olsen, A.J. (1998). Automated docking using a Lamarckian genetic algorithm and an empirical binding free energy function. J. Comput. Chem. *19*, 1639–1662.
31. Kuo, C.-J., Chi, Y.-H., Hsu, T.-A., and Liang, P.-H. (2004). Characterization of SARS main protease and inhibitor assay using a fluorogenic substrate. Biochem. Biophys. Res. Commun. *318*, 862–867.
32. Hsu, M.-F., Kuo, C.-J., Chang, K.-T., Chang, H.-C., Chou, C.-C., Ko, T.-P., Shr, H.-L., Chang, G.-G., Wang, A.H.-J., and Liang, P.-H. (2005). Mechanism of the maturation process of SARS-CoV 3CL protease. J. Biol. Chem. *280*, 31257–31266.